

Article

A Kinetic Study of a Photo-Oxidation Reaction between α -Terpinene and Singlet Oxygen in a Novel Oscillatory Baffled Photo Reactor

Jianhan Chen, Rohen Prinsloo  and Xiongwei Ni * 

Centre for Oscillatory Baffled Reactor Advancement, School of Engineering and Physical Sciences, Heriot-Watt University, Edinburgh EH14 4AS, UK

* Correspondence: x.ni@hw.ac.uk; Tel.: +44-1314513781

Abstract: By planting LEDs on the surfaces of orifice baffles, a novel batch oscillatory baffled photoreactor (OBPR) together with polymer-supported Rose Bengal (Ps-RB) beads are here used to investigate the reaction kinetics of a photo-oxidation reaction between α -terpinene and singlet oxygen ($^1\text{O}_2$). In the mode of NMR data analysis that is widely used for this reaction, α -terpinene and ascaridole are treated as a reaction pair, assuming kinetically singlet oxygen is in excess or constant. We have, for the first time, here examined the validity of the method, discovered that increasing α -terpinene initially leads to an increase in ascaridole, indicating that the supply of singlet oxygen is in excess. Applying a kinetic analysis, a pseudo-first-order reaction kinetics is confirmed, supporting this assumption. We have subsequently initiated a methodology of estimating the $^1\text{O}_2$ concentrations based on the proportionality of ascaridole concentrations with respect to its maximum under these conditions. With the help of the estimated singlet oxygen data, the efficiency of $^1\text{O}_2$ utilization and the photo efficiency of converting molecular oxygen to $^1\text{O}_2$ are further proposed and evaluated. We have also identified conditions under which a further increase in α -terpinene has caused decreases in ascaridole, implying kinetically that $^1\text{O}_2$ has now become a limiting reagent, and the method of treating α -terpinene and ascaridole as a reaction pair in the data analysis would no longer be valid under those conditions.



Citation: Chen, J.; Prinsloo, R.; Ni, X. A Kinetic Study of a Photo-Oxidation Reaction between α -Terpinene and Singlet Oxygen in a Novel Oscillatory Baffled Photo Reactor. *Technologies* **2024**, *12*, 29. <https://doi.org/10.3390/technologies12030029>

Academic Editor: Mohammednoor Altarawneh

Received: 13 December 2023

Revised: 2 February 2024

Accepted: 8 February 2024

Published: 21 February 2024



Copyright: © 2024 by the authors. Licensee MDPI, Basel, Switzerland. This article is an open access article distributed under the terms and conditions of the Creative Commons Attribution (CC BY) license (<https://creativecommons.org/licenses/by/4.0/>).

Keywords: photo-oxidation; singlet oxygen; reaction kinetics; reaction mechanism; oscillatory baffled photoreactor

1. Introduction

Heterogeneous photo-aided reactions and photocatalysis are initiated by the absorption of light. Scalable uniform mixing in handling multiphases and scalable uniform light distribution in providing light sources are the two most critical requirements in photoreactors, so much so that the scalability of photoreactors has been identified as a key challenge in photochemical transformations in the chemical industry [1]. In terms of light provision, UV lamps/bars are traditionally placed outside or within reactors, suffering from the non-uniform distribution of light intensity, and low power-to-photon efficiency and scale-up ability [2,3]. LEDs, on the other hand, offer a much narrower spectrum of light for targeted reactions and are sufficiently small to be installed within reactors, enabling uniform light distributions. LEDs have thus become the main light source in most of the lab-scale photoreactors.

In terms of mixing, the century-old problem remains whereby mixing gets worse with increasing scales: simply scaling up stirred tank reactors does not meet the above critical needs. Microreactors are seen as viable alternatives in solving the mixing issues, allowing the safe exploitation of hazardous materials, while enabling optimal irradiance due to their narrow dimensions. Subsequently, a wide range of photochemistry applications using a variety of flow reactors have been reported in recent years [1,4–8].

While lab-scale flow photoreactors are sufficient to produce small quantities of targeted molecules [9], applications in industrial-scale photochemical processes are comparatively rare due to the generally poor economics, complex scalability and safety issues of many photochemical transformations [10]. There are currently three main strategies used in scaling up photo-microreactors: numbering up, lengthening the channel or increasing channel diameter [11]. Numbering up is a method of adding reactor systems in parallel until a desired productivity of chemicals is achieved. However, high inventory costs are a major drawback, as multiple pumps, mass flow controllers and reactors are required [12,13]. Lengthening the flow path while keeping the channel diameter constant enables faster flow velocities while maintaining the same photon flux, but leads to issues with large pressure drops over the reactor [14]. Increasing diameter is the least viable method in scaling up microchannel reactors, as it weakens/diminishes diffusion-driven mixing in the reactor [15,16], providing poorer scale up than the former methods.

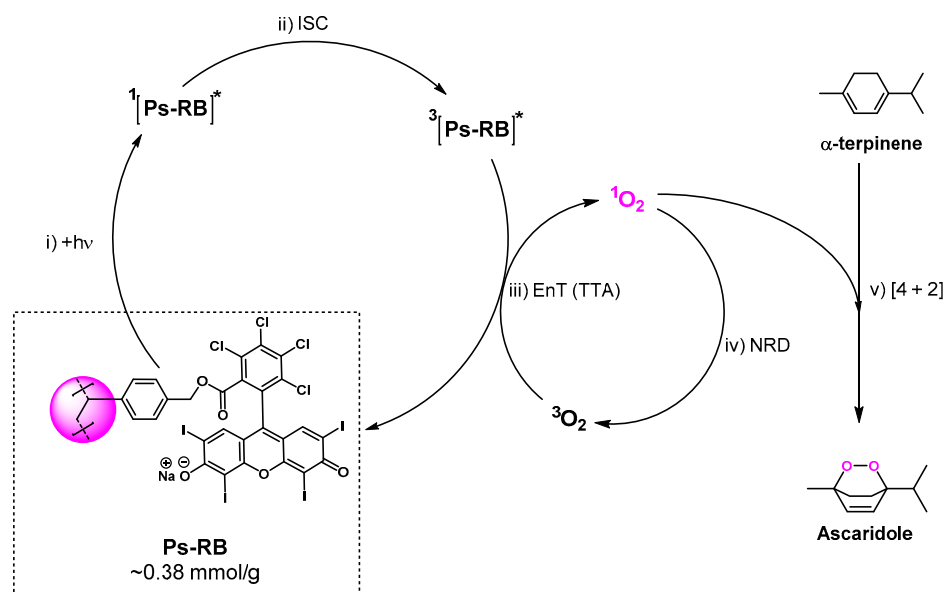
In this study, we present a novel batch oscillatory baffled photo reactor (OBPR) that provides uniform mixing and solid suspension via the succession and cession of eddies. Orifice baffles are one of the key intrinsic elements of the reactor set-up; planting LEDs on the surfaces of orifice baffles [17] enables uniform and controllable light distribution/intensity. The scale-up of this device is achieved through continuous oscillatory baffled reactors (COBR) that have a number of unique offerings: (a) plug flow mixing is generated in laminar flows, minimizing pressure drop and allowing longer residence times [18–21]; (b) uniform mixing is scalable [22,23]; (c) COBRs are good in handling solids [24,25] and have been implemented in industrial applications [26], meeting both critical requirements in photoreactors. The work to be presented in this paper is only associated with batch OBPRs. Using a model photo-oxidation reaction between α -terpinene and singlet oxygen ($^1\text{O}_2$), we report our kinetic analysis and assessment of the reaction. Polymer-supported Rose Bengal beads are used in the work, because the OBPR has the excellent capability of suspending solids and enabling uniform light absorption.

2. The Reaction Scheme and Experimental Set Up

2.1. Reaction Scheme

The photo-oxidation reaction is shown in Scheme 1 with polymer-supported Rose Bengal (Ps-RB) porous beads as the heterogeneous photosensitizer. The beads were synthesized in house and characterized according to known literature methods [27,28]. The first step of the reaction involves photo absorption ($+h\nu$) by the Ps-RB chromophore promoting an electron to a higher-order singlet electronic excited state ($^1[\text{Ps-RB}]^*$); $^1[\text{Ps-RB}]^*$ converts to a triplet excited state ($^3[\text{Ps-RB}]^*$) via intersystem crossing (ISC), which is the second step; the energy transfer (EnT) from $^3[\text{Ps-RB}]^*$ to ground-state triplet molecular oxygen ($^3\text{O}_2$) then occurs via triplet-triplet annihilation (TTA), to return the Ps-RB to their initial ground state and produce $^1\text{O}_2$; the next step is that $^1\text{O}_2$ spontaneously decomposes to $^3\text{O}_2$ via non-radiative decay (NRD) through vibronic energy transfer with solvent molecules, and $^1\text{O}_2$ encounters α -terpinene in solution and undergoes a productive [4 + 2] cycloaddition to yield the endoperoxide product, ascaridole, known as a Diels–Alder-type reaction (Scheme 1). 1,3-Dienes commonly undergoes [4 + 2] cycloaddition reactions with singlet oxygen $^1\text{O}_2$ to yield endoperoxides. This reaction has been extensively studied on naphthalene derivatives [29–31]. Other chemical transformations such as [2 + 2] additions or “ene”-type reactions are also possible, forming dioxetanes and hydroperoxides, respectively [32]. $^1\text{O}_2$ exists as a gas, but is dissolved in the reaction mixture or solvent [33]. Singlet oxygen is unstable, and its lifetime changes dramatically in different solvents, ranging from 4 to 628 μs [34], depending on the efficiency of energy transfer from electronic to intramolecular vibrational states; for instance, the lifetime in water is one order of magnitude lower than that in deuterated water. Chloroform (CHCl_3) provides the longest $^1\text{O}_2$ lifetime ($\sim 90 \mu\text{s}$) of all common, non-deuterated laboratory solvents [35], and so was chosen as the solvent in this study. It should be noted that the amount of ascaridole produced does

not equal the amount of $^1\text{O}_2$ formed due to non-radiative decay, but what is certain is that the formation of ascaridole is direct evidence of the existence of singlet oxygen [2].



Scheme 1. Reaction scheme of singlet oxygen ($^1\text{O}_2$) photosensitization by polymer-supported Rose Bengal (Ps-RB) and subsequent photo-oxidation of α -terpinene to produce ascaridole (courtesy of Christopher Thomson).

Heterogeneous photosensitizers have many advantages over their homogeneous counterparts; for example, they are readily prepared and are easily removed post-reaction, and when suspended in solution, they do not accumulate or clog reactors. Heterogeneous photosensitizers are generally composed of organic dyes bearing a (hetero)aromatic core, e.g., Rose Bengal (RB). Because RB suffers from extensive photobleaching/degradation under prolonged irradiation, the leakage is usually difficult to remove from reaction effluents [36,37], and so modifications in synthesis have led to various robust solid photosensitizers. Previously, a versatile organic dye, 4,4-difluoro-4-bora-3a,4a-diaza-s-indacene (BODIPY), with polymer support was used as the photosensitizer in the same reaction, with nitrogen- and boron-containing heterocycles [9] with high fluorescence quantum yields and significant visible light absorption; the ideal light wavelength fell between 500 and 540 nm. In this work, polymer-supported Rose Bengal (Ps-RB) porous beads are used; they show high absorption coefficients in the visible spectral region and are stable after photosensitization. Their optimal light wavelength is 530 nm [38]. The key advantage of Ps-RB over BODIPY is that the maximum absorbance wavelength is red-shifted and requires lower energy, reducing the likelihood of the photodecomposition of reactants and products [39].

2.2. Materials

α -terpinene was purchased from the Division of Tokyo Chemical Industry (TCI) (>90% purity); all organic solvents and reagents were sourced from Fisher Scientific (Bishop Meadow Road, Loughborough, Leicestershire, LE11 5RG, UK) at SLR grade, and were used as received without further purification unless otherwise stated.

2.3. Reactor Setup

The OBPR consists of a glass column of 50 mm in diameter and 480 mm in height, as shown in Figure 1. The volume of the reactor is 600 mL, with the working volume of 500 mL. Orifice baffles have an outer diameter of 46 mm, a hole diameter of 26 mm and a baffle spacing of 60 mm. Each set comprises three orifice baffles; each baffle has 6 evenly spaced green LEDs (Cree 5 mm round LEDs) planted on the lower surface (can also be

both sides), as shown in Figure 1, for the purpose of providing light. The provision of light in the OBPR differs from traditional means. Firstly, the LEDs are placed within the reactor, directly in contact with reaction medium, thus enhancing the intensity of light supply; secondly, the LEDs move with the baffle plates up and down the column, and the light radiation covers the whole reactor area, but far fewer LEDs are required; thirdly, whole-area illumination is not achieved, as in many microreactor systems, and much less energy is used, meaning that less heat is generated (the latter is an important factor for some chemical or biological compounds that can be decomposed with excessive heat). The leads of LEDs are covered by epoxy resin, which provides insulation, material compatibility and corrosion resistance. The wavelength and light intensity of the green LEDs are 530 nm and 0.756 watts, respectively, and the intensity of the radiation is estimated at 29 W/m^2 . An air sparger is located at the base of the OBPR for introducing air at a controlled rate.

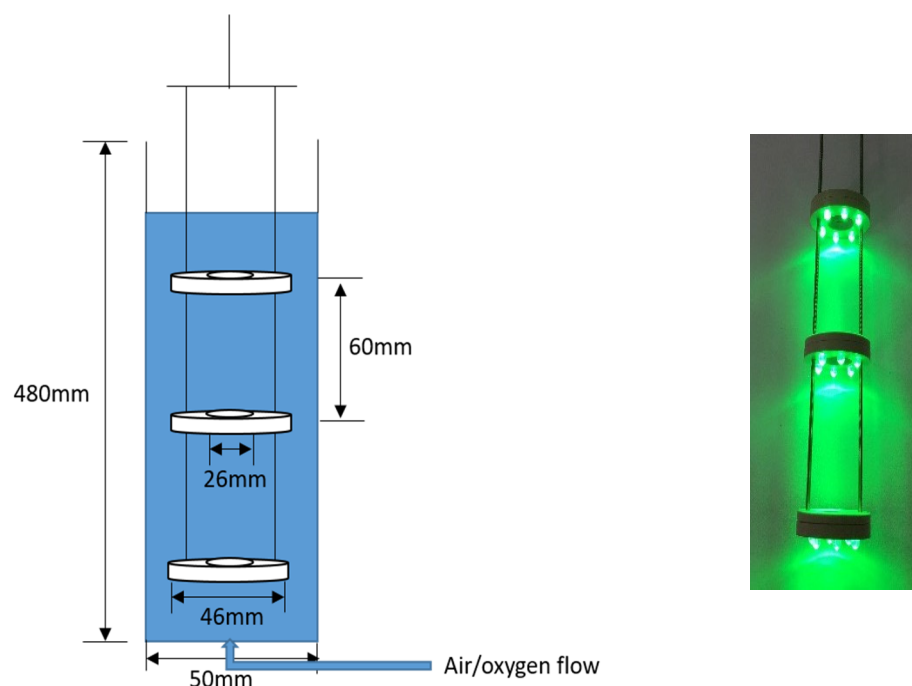


Figure 1. The schematics of the OBPR reactor and orifice baffles with LEDs.

Based on a previous work in a microchannel reactor [11,13], about 390 mL CHCl_3 was mixed with 4.225 mL of α -terpinene in the OBPR in the presence of Ps-RB beads of 1600 mg. A constant liquid volume of 400 mL was maintained for all experiments. The oscillation frequency and amplitude were switched on once all chemicals were charged into the OBPR; the reaction was initiated when the LEDs were turned on, and the duration of the reaction was 120 min. The Ps-RB beads of 100 μm mean size were uniformly suspended and kept within the OBPR under the selected oscillation conditions. A lid was placed on the top of the OBPR to prevent volatile matter from escaping. Runs were repeated to ensure data repeatability and reliability (see Table 1), and averaged values have been used in the following data presentations.

2.4. Analytic Method

Samples were taken regularly and analyzed using proton nuclear magnetic resonance (^1H NMR) to determine the composition/concentration of the mixture. The procedure of treating the samples was as follows:

- Each 2 mL sample containing $\text{CHCl}_3 + \alpha$ -terpinene + ascaridole was injected into a dark vial to stop the reaction (reaction stops when light is off);

- The sample was placed in a round-bottom flask and the solvent (CHCl_3) was removed under reduced pressure on a rotary evaporator ($40\text{ }^\circ\text{C}$, 365 mbar for ~ 5 min);
- The oily residue was dissolved in 0.5 mL of deuterated chloroform (CDCl_3) and a ^1H NMR was obtained (300 MHz Bruker AVIII spectrometer);
- Peaks in the region between 6.70 and 5.40 ppm were used to determine the conversion of α -terpinene and the appearance of ascaridole.

Figure 2 shows typical ^1H NMR spectra in chloroform-*d*, showing the alkenyl proton resonances of α -terpinene as a multiplet at 5.61 ppm, and ascaridole as a doublet-of-doubles centered at 6.45 ppm, consistent with previous reports [40]. The resonance signals count for two alkenyl protons of the respective molecules. While p-cymene is a byproduct in the reaction, it is not detected by the ^1H NMR, which is consistent with other studies [41]. At the reaction stoichiometric ratio of 1:1, the integrals of these signals are directly proportional to the relative concentrations of the two species. The concentration of α -terpinene at time t ($C_{\alpha\text{T}}$) is the ratio of the integrated NMR area of α -terpinene at time t ($\text{Area}_{\alpha\text{T}}$) over its corresponding area at time $t = 0$ (taking as 100), multiplied by its initial concentration at $t = 0$ ($C_{\alpha\text{T}0} = 0.051917$ mol/L). The concentration of ascaridole (C_{As}) is then the ratio of the integrated area of ascaridole over the total area at time t multiplied by the initial concentration of α -terpinene, since the initial concentration of ascaridole at $t = 0$ is zero, as:

$$C_{\alpha\text{T}} = \left(\frac{\text{Area}_{\alpha\text{T}}}{\text{Area}_{\alpha\text{T}0}} \right) C_{\alpha\text{T}0} \quad C_{\text{As}} = \left(\frac{\text{Area}_{\text{As}}}{\text{Area}_{\text{As}} + \text{Area}_{\alpha\text{T}}} \right) C_{\alpha\text{T}0} \quad (1)$$

The byproduct is not detectable, $\text{Area}_{\text{As}} + \text{Area}_{\alpha\text{T}} = 100$, which makes the concentration of ascaridole a reaction pair with that of α -terpinene. The reaction conversion rate is typically about 20% that is far less than the quantum yields shown in Table 2.

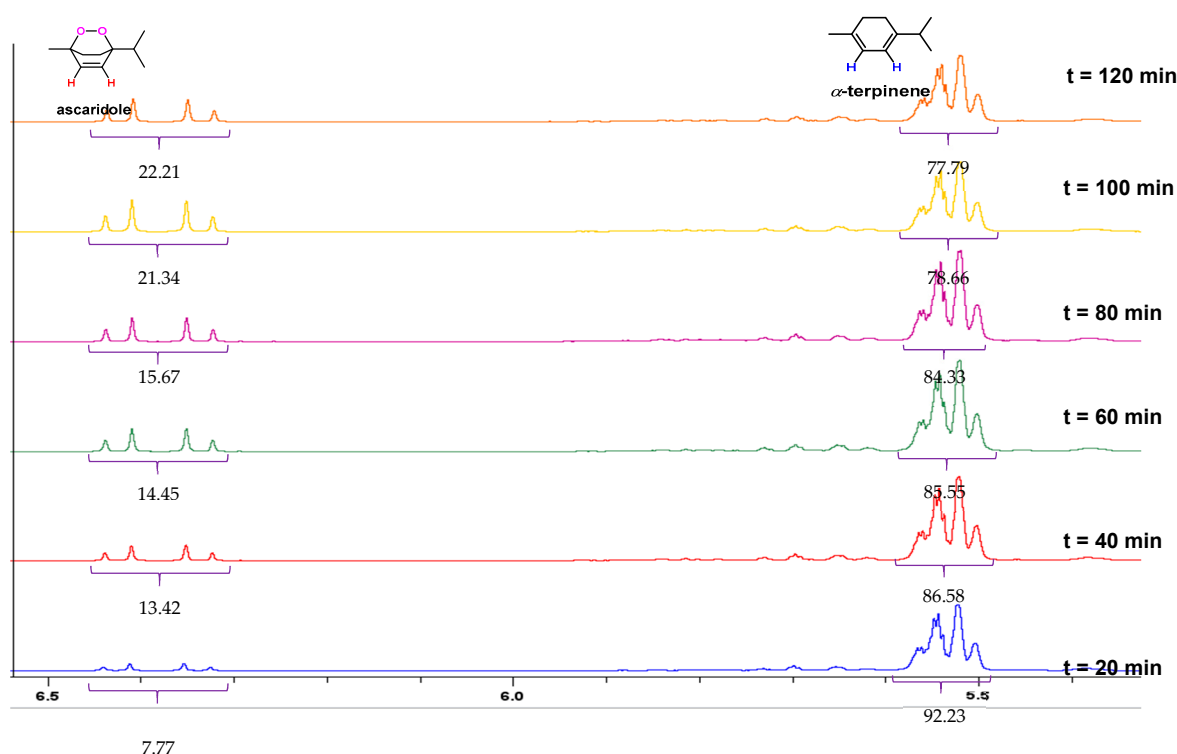


Figure 2. Stacked ^1H NMR spectra for monitoring the conversion of the two alkenyl protons of α -terpinene to ascaridole at an interval of 20 min in the OBPR. Photo-oxidation conditions: mass of Ps-RB = 800 mg, irradiation wavelength = 530 nm, oscillation frequency = 2.5 Hz, oscillation amplitude = 24 mm, air flow rate = 172.5 mL/min.

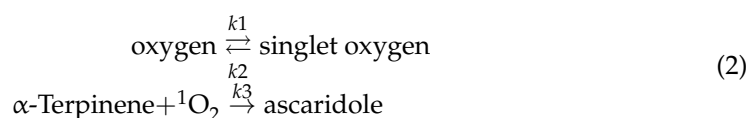
Table 1. Experimental conditions (bead mass = 1600 mg, irradiation wavelength = 530 nm, oscillation frequency = 2.5 Hz, oscillation amplitude = 24 mm, air flow rate = 172.5 mL/min, duration = 120 min).

| Run Number | Chloroform (mL) | α -Terpinene (mL) | Number of Repeated Runs |
|------------|-----------------|--------------------------|-------------------------|
| 1 | 397.88 | 2.12 | 1 |
| 2 | 395.77 | 4.23 (default) | 2 |
| 3 | 393.00 | 7.00 | 2 |
| 4 | 391.53 | 8.47 | 3 |
| 5 | 390.00 | 10.00 | 2 |
| 6 | 383.10 | 16.90 | 2 |
| 7 | 374.50 | 25.50 | 3 |

3. Results and Discussion

3.1. Kinetic Assessment

The overall reaction in Scheme 1 can be described by a sequence of two reactions:



Following the reaction Scheme 1, some singlet oxygen (${}^1\text{O}_2$) decomposes to molecular oxygen (${}^3\text{O}_2$) via non-radiative decay (NRD)—the first part of the reversible reaction accounts for this process. At a fixed oscillatory frequency (f) and amplitude (x_0) in the OBPR with a known quantity of polymer-supported Rose Bengal beads at continuous controlled light irradiation under a steady state, a net amount of ${}^1\text{O}_2$ (resulting from the first part of the reaction) is generated and reacts with α -terpinene to produce ascaridole (the second part of the reaction). For one equivalent each of ascaridole and α -terpinene without any byproduct, the data analysis focuses on the consumption of α -terpinene as a reaction pair of the generation of ascaridole. This effectively assumes that the concentration of singlet oxygen is kinetically either in excess or constant. To the authors' knowledge, no research publications have looked into this matter. In order to testify to and verify this assumption, a number of planned experiments were carried out using different amounts of α -terpinene and chloroform while keeping the same reaction volume—see Table 1. Note that Run 2 was the default condition, based on previous studies [9,42,43].

Figure 3 compares the concentration profiles of ascaridole with different amounts of α -terpinene. An increase in the concentration of ascaridole as a function of time can be seen with the increase in α -terpinene in Figure 3a on the left (the filled symbols). This indicates that ${}^1\text{O}_2$ supply in the OBPR is indeed in excess. Further increases in the reagent, however, have brought about reductions in the product (see the open symbols) shown in Figure 3b on the right, implying that under these experimental conditions, ${}^1\text{O}_2$ has become the limiting reagent; the concentration of ascaridole would be solely dependent upon the concentration of ${}^1\text{O}_2$, instead of α -terpinene. This stipulates that the widely used method of treating α -terpinene and ascaridole as a reaction pair, as shown in Equation (1), would no longer be valid under these conditions. Note that chloroform is the solvent that does not participate in the reaction and is present at significant excess over α -terpinene. Its effect on the concentration of ascaridole should be minimal, but this has not been tested.

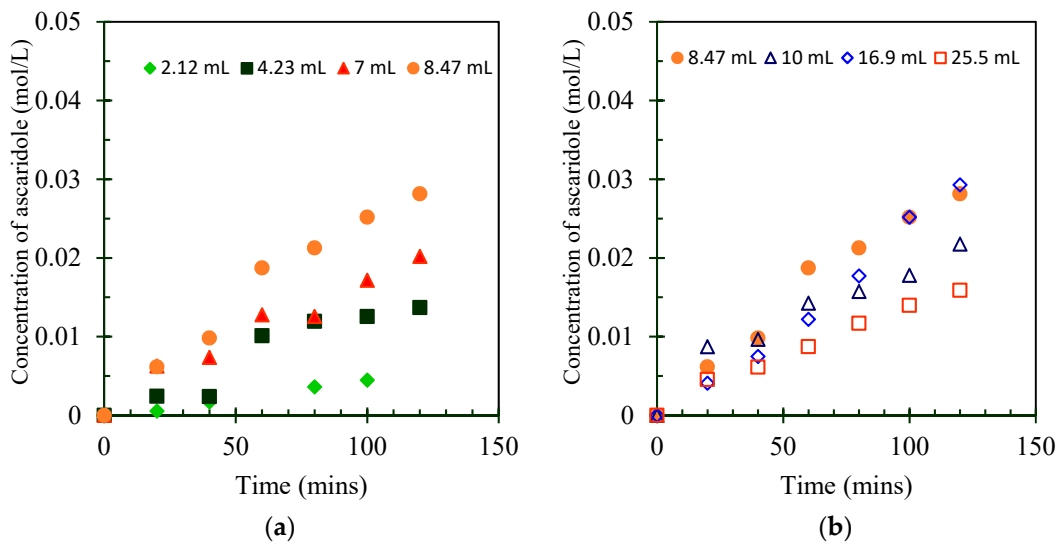


Figure 3. Concentrations of ascaridole for different volumes of α -terpinene (bead mass = 1600 mg, irradiation wavelength = 530 nm, oscillation frequency = 2.5 Hz, oscillation amplitude = 24 mm, air flow rate = 172.5 mL/min, duration = 120 min).

Under conditions where $^1\text{O}_2$ is in excess (Figure 3a), the second-order reaction of $^1\text{O}_2 + \alpha$ -terpinene $\xrightarrow{k_3}$ ascaridole is then reduced to a pseudo-first-order reaction of α -terpinene $\xrightarrow{k_3}$ ascaridole. It is then justified to treat the two as a reaction pair. The rate equation and the integral form are given below:

$$-\frac{dC_{aT}}{dt} = k_3 C_{aT} \quad \ln\left(\frac{C_{aT0}}{C_{aT}}\right) = k_3 t \quad (3)$$

When plotting $\ln\left(\frac{C_{aT0}}{C_{aT}}\right)$ vs. time for α -terpinene at 2.12, 4.23 and 7 mL, approximate straight lines can be seen in Figure 4, verifying the pseudo-first-order kinetics with an averaged rate constant of 0.0020/min.

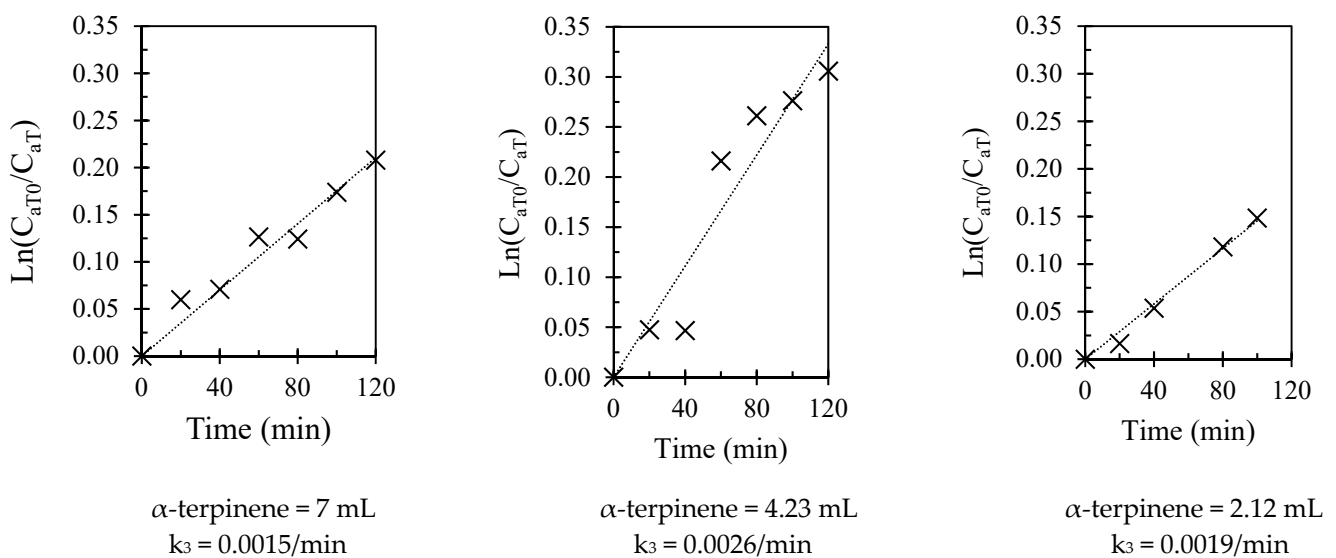


Figure 4. Fitting for pseudo-first-order kinetics (bead mass = 1600 mg, irradiation wavelength = 530 nm, oscillation frequency = 2.5 Hz, oscillation amplitude = 24 mm, air flow rate = 172.5 mL/min, duration = 120 min).

When 8.5 mL of α -terpinene is used, the conversion of ascaridole reaches its maximum, implying that neither singlet oxygen nor α -terpinene is in excess. Using the proportionality of ascaridole with respect to its maximum at 8.5 mL, shown in Figure 3a, the excess $^1\text{O}_2$ concentrations derived with 7/4.23/2.12 mL of α -terpinene can be estimated using the equation below, taking 7 mL as an example:

$$C_{O_2^1} = \left[1 + \frac{(C_{As})_{8.47\text{ml}} - (C_{As})_{7\text{ml}}}{(C_{As})_{8.47\text{ml}}} \right] \times C_{\alpha T} \quad (4)$$

Figure 5 shows the concentrations of all species for the three volumes of α -terpinene. Note that there are no data of $^1\text{O}_2$ at $t = 0$; this is due to the concentration of ascaridole being zero at the start, and $^1\text{O}_2$ concentrations were only estimated from 20 min onwards. We see that the concentrations of singlet oxygen are greater than those of α -terpinene, demonstrating that $^1\text{O}_2$ is in excess under those conditions. We also note that the concentration of $^1\text{O}_2$ remains more or less unchanged with each measure of α -terpinene, which is consistent with what was stated earlier—that a net amount of $^1\text{O}_2$ is generated in the OBPR under a steady state.

By feeding the data on α -terpinene, ascaridole and k_3 (from Figure 4) into the reaction kinetic model in COPASI (Complex Pathway Simulator), the concentrations of singlet oxygen can be reconstructed as shown in Figure 5 (filled symbol). Note that COPASI is a versatile modeling tool that can be used for model development, model simulations (such as stochastic simulations and differential equation simulations), numerous sorts of analyses (such as sensitivity analysis, parameter estimation, and metabolic control analysis) and kinetic extraction [44]. We see that the $^1\text{O}_2$ concentrations estimated using the proportionality of ascaridole at different amounts of α -terpinene (open triangles) match reasonably well with those determined using the kinetic model (filled triangles). This further validates our proposed methodologies. We note that zero-order reaction kinetics were reported by other studies for this reaction [41,45,46]; the presence of zeroth order kinetics indicates that the reaction rate is a sole function of the reaction rate constant, and does not depend on the concentrations of reagents. When we vary the concentrations of α -terpinene, the dependence of the reaction rate on the concentrations of the reagent is clearly demonstrated.

Thanks to the data on $^1\text{O}_2$ that we estimated, we can also evaluate the efficiency of $^1\text{O}_2$ utilization using the definition below, even when it is in excess:

$$\text{Efficiency of singlet oxygen utilization (\%)} = 100\% - \frac{\text{Singlet oxygen} - \text{ascaridole}}{\text{Singlet oxygen}} \quad (5)$$

The efficiencies of $^1\text{O}_2$ utilization are tabulated in Table 2 for measures of α -terpinene from 2.12 to 7 mL.

Table 2. Average efficiency of $^1\text{O}_2$ utilization and efficiency of photo conversion for three volumes of α -terpinene (photosensitizer = 1600 mg, irradiation wavelength = 530 nm, $f = 2.5$ Hz, $x_0 = 24$ mm, air flow = 172.5 mL/min, duration = 120 min).

| α -Terpinene (mL) | Efficiency of $^1\text{O}_2$ Utilization (%) | Efficiency of Photo Conversion (%) | Apparent Quantum Yield (%) |
|--------------------------|--|------------------------------------|----------------------------|
| 7 | 10.7 | 0.10 | 87 |
| 4.23 | 14.6 | 0.07 | 57 |
| 2.12 | 4.9 | 0.06 | 19 |

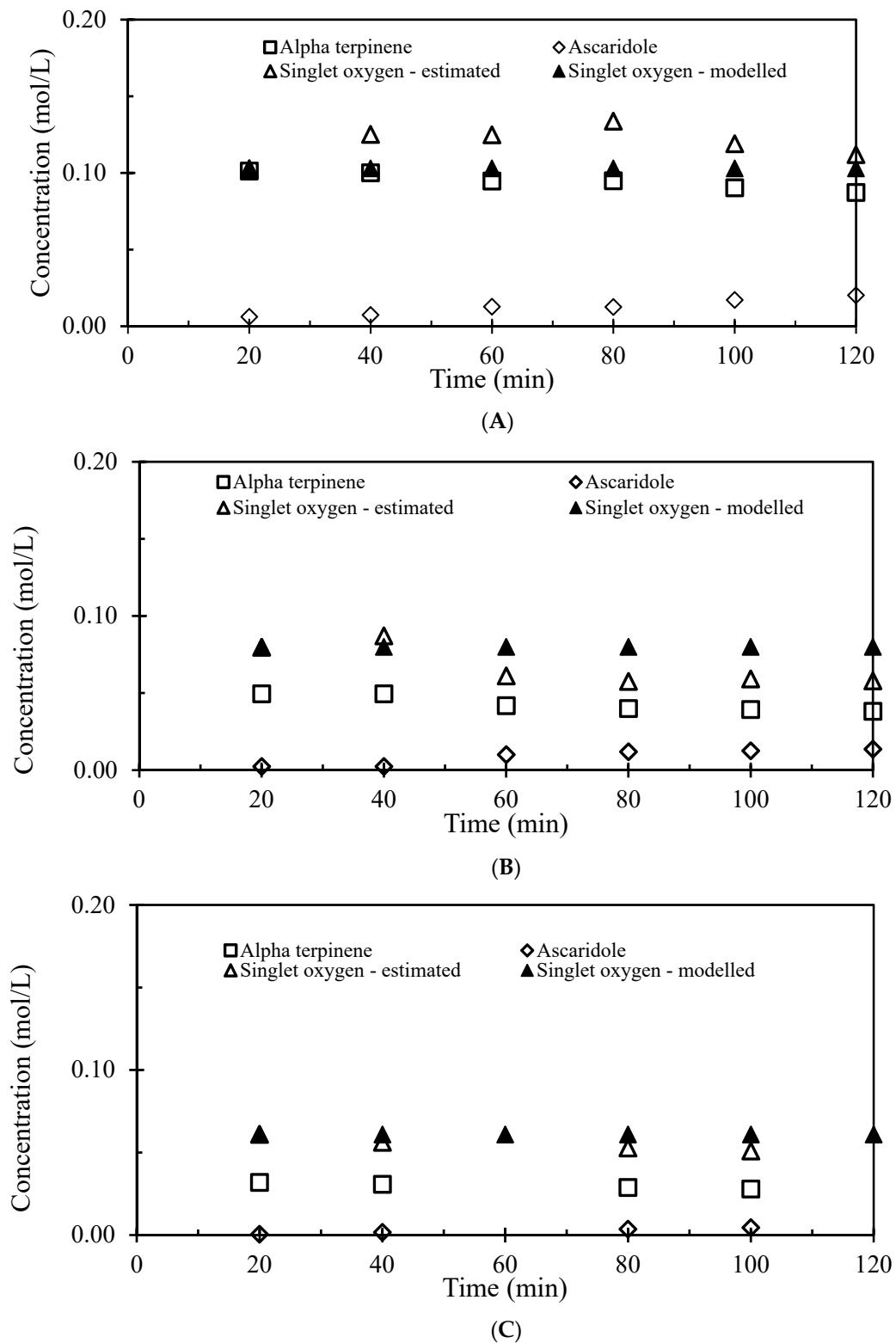


Figure 5. Estimated singlet oxygen concentrations (bead mass = 1600 mg, irradiation wavelength = 530 nm, oscillation frequency = 2.5 Hz, oscillation amplitude = 24 mm, air flow rate = 172.5 mL/min). (A) α -terpinene = 7 mL; (B) α -terpinene = 4.23 mL; (C) α -terpinene = 2.12 mL.

3.2. The First Step of the Reaction

The process of conversion from molecular oxygen to $^1\text{O}_2$ in the first part of the overall reaction in Equation (2) relies on photo-elevation/energy transfer. Due to a significant

energy barrier (94 kJ/mol), $^3\text{O}_2$ molecules cannot directly be excited to $^1\text{O}_2$ due to this electronic transition being forbidden by spin selection rules; this process therefore requires a triplet photosensitiser to enable the triplet–triplet annihilation energy transfer mechanism [47]. When photons of the correct wavelength (<600 nm) irradiate the Ps-RB beads, the supported Rose Bengal chromophore is electronically excited and enters into a triplet state via intersystem crossing (ISC), which enables it to undergo an energy transfer, resulting in a triplet–triplet annihilation process with oxygen to produce singlet oxygen [48]. The very short lifetime of singlet oxygen depends on the temperature and solvent environment, as vibronic energy transfer with a solvent is a competitive, non-productive process that returns $^1\text{O}_2$ to its ground state, $^3\text{O}_2$ [49], which is the first part of the overall reaction. The question remains as to whether the molecule oxygen is an oxygen gas molecule [50,51] or dissolved oxygen. Air/oxygen is generally sparged into the reactor; as a result, a significant amount of gas bubbles exit the reactor without participating in the reaction, due to the density difference, the buoyance effect, and critically, the lack of a mixing mechanism that can hold the bubbles within a traditional reactor. This suggests that $^3\text{O}_2$ is associated with dissolved oxygen. The process of converting oxygen gas to dissolved oxygen in chloroform is a mass transfer-controlled process, and is mainly affected by mixing and air flow rate, determined by novel reactor designs. The properties of mixing in the OBPR are governed by the oscillatory Reynolds number [20] (Re_o) and the Strouhal number (St), defined as:

$$Re_o = \frac{2\pi f x_0 \rho D}{\mu} \quad St = \frac{D}{4\pi x_0} \quad (6)$$

where D is the tube diameter (m), ρ is the fluid density (kg m^{-3}), x_0 is the center-to-peak amplitude (m), μ is the viscosity (Pa s) and f is the oscillatory frequency (Hz). The oscillatory Reynolds number is related to the intensity of mixing, while the Strouhal number indicates the degree of eddy propagation [20,25]. The effects of the mixing (oscillation amplitude, or St) and [1] air flow rates on the conversion of ascaridole are given in Figure 6.

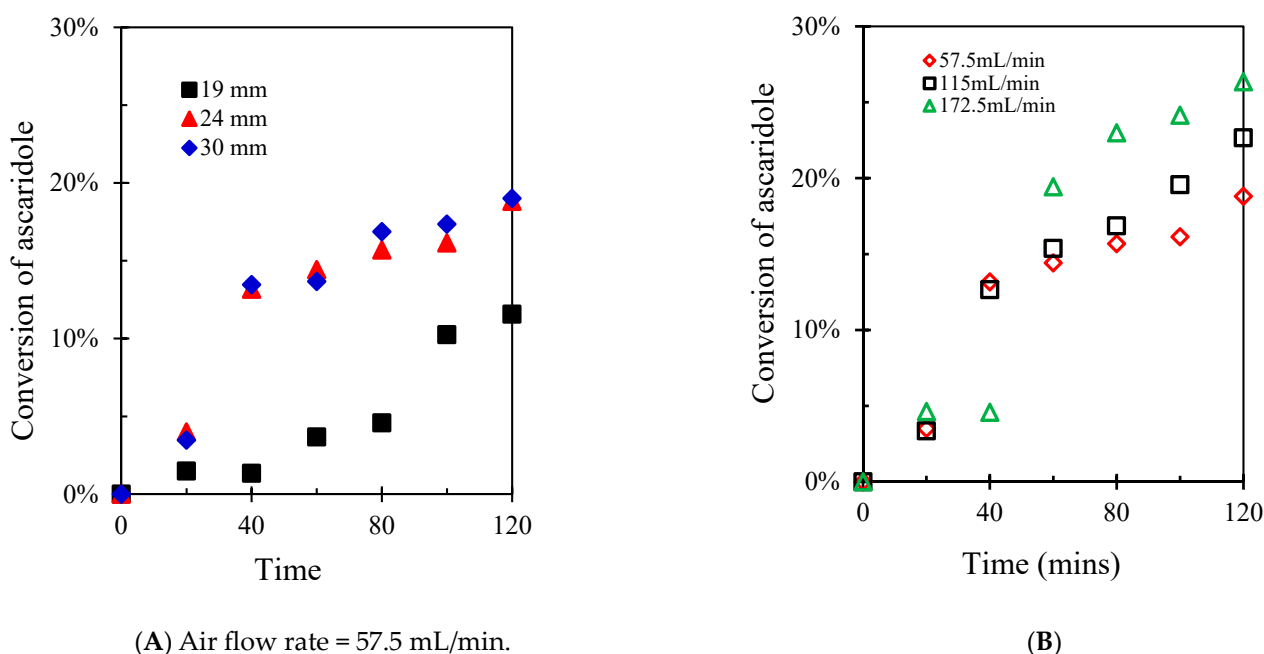


Figure 6. Conversion of ascaridole at different oscillation amplitudes (A) and air flow rates (B) (bead mass = 1600 mg, irradiation wavelength = 530 nm, oscillation frequency = 2.5 Hz, oscillation amplitude = 24 mm).

We see that, generally, the higher the oscillation, the greater the conversion (Figure 6A). As mixing intensity increases in the OBPR and becomes uniform, it breaks up bubbles,

leading to a decrease in bubble sizes and an increase in bubble surface area; these bubbles are trapped in the vortices for longer periods of time, enhancing the residence time required for mass transfer within the reactor [52]. The direct result is an increase in dissolved oxygen concentration in the solvent [53] and more excited molecular oxygen, which means more $^1\text{O}_2$. The degree of improvement in the conversion is, however, rather limited for all amplitudes. The effect of air flow rate on the conversion (Figure 6B) tells a similar story—the higher the air flow rate, the greater the conversion. However, there is an operational limit for further increasing air flow rate, as channeling takes place, thus extracting the beads from the OBPR. The highest flow rate was used in our kinetics studies.

By comparing the total amount of air/oxygen sparged into the OBPR with the estimated amount of $^1\text{O}_2$ every 20 min, the efficiency of the photo conversion of $^1\text{O}_2$ can be evaluated as

$$\text{Efficiency of photo conversion of singlet oxygen (\%)} = 100\% - \frac{\text{Oxygen input} - \text{Singlet oxygen}}{\text{Oxygen input}} \quad (7)$$

The oxygen input is calculated using the air flow rate (21% oxygen) and the duration in time; the $^1\text{O}_2$ concentration is then converted into mass for the same duration. Table 2 summarizes both efficiencies. Using Max Planck's equation ($E = h C/\lambda$), we can calculate the energy of one photon at the wavelength of 530 nm, where h is the Planck's constant (6.626×10^{-34} J s), C the speed of light (3×10^8 m) and λ the wavelength of radiation (530 nm = 0.53×10^{-6} m). We thus have $E = 3.75 \times 10^{-19}$ J.

For a typical experimental duration of 120 min, the energy released by the LEDs is $0.756 \text{ J/s} \times 120 \text{ min} \times 60 \text{ s} = 5443.2 \text{ J}$, meaning that the number of photons is $5443.2 \text{ J}/3.75 \times 10^{-22} \text{ J} = 1.45 \times 10^{22}$. The apparent quantum yield is equal to the number of reacted molecules divided by the number of photons sent. Taking the 7 mL measure of α -terpinene as an example, the initial and final concentrations of α -terpinene were 0.108 mol/L and 0.0873 mol/L, respectively, implying that the quantity of reacted α -terpinene was 0.0207 mol/L. The number of molecules per L was thus $0.0207 \times 6.02 \times 10^{23}$ (the Avogadro's number) = 1.246×10^{22} , implying an apparent quantum yield of $1.246 \times 10^{22}/1.45 \times 10^{22} = 87\%$. The apparent quantum yields for two other conditions are shown in Table 2.

The limited conversion to ascaridole shown in Figures 5 and 6 is the direct result of the combined low efficiency of $^1\text{O}_2$ utilization with the very low efficiency of conversion of $^3\text{O}_2$ to $^1\text{O}_2$, the latter being perhaps the greatest obstacle for this reaction (indeed for most photo-aided and photocatalysis reactions). The low conversion to ascaridole seen here is also consistent with the results of previous work, although these used BODIPY as the photosensitizer [43]. We are in the process of expanding this work to determine the pressure dependence of $^1\text{O}_2$ by varying the partial pressures, and we are also looking into using a dissolved oxygen probe to measure the concentration of dissolved oxygen to enable better evaluations of photo conversion from molecular oxygen to singlet oxygen.

4. Conclusions

Four novel results are reported in this paper. Firstly, expanding on the success of continuous oscillatory baffled reactor technology, we have here introduced a novel batch oscillatory baffled photoreactor (OBPR) with LEDs planted evenly on the surfaces of the orifice plates, allowing uniform and controlled light distribution for photo-aided reactions and photocatalysis from the laboratory to full scales. Secondly, using a model photo-oxidation reaction with a solid photosensitizer, we have carried out a full examination of the validity of treating α -terpinene and ascaridole as a reaction pair in the commonly used mode of NMR data analysis. We have revealed that increasing α -terpinene initially leads to an increase in ascaridole, implying that the supply of singlet oxygen will be in excess. When applying pseudo-first-order reaction kinetics, the results fully support this hypothesis, validating the data analysis performed under these conditions. Further increases in α -terpinene, however, led to reductions in ascaridole, kinetically implying that

$^1\text{O}_2$ has become the limiting reagent. The method of treating α -terpinene and ascaridole as a reaction pair for the data analysis would thus no longer be valid under these conditions. Thirdly, we have developed a method of estimating the concentrations of $^1\text{O}_2$ using the concentration profiles of ascaridole with respect to its maximum. The presence of excess $^1\text{O}_2$ is demonstrated in each of the α -terpinene volumes. Knowing the concentrations of α -terpinene and ascaridole, together with the rate constant, we have reconstructed the $^1\text{O}_2$ concentrations, which match reasonably well with the estimated values. Lastly, using the estimated $^1\text{O}_2$ data, we have here proposed a methodology of evaluating the efficiency of $^1\text{O}_2$ utilization and the photo efficiency of the conversion of $^3\text{O}_2$ to $^1\text{O}_2$. The combination of the above two deficiencies led to the overall low conversion of ascaridole (~20%) in this photo-oxidation experiment.

Author Contributions: Conceptualization, X.N.; Methodology, J.C., R.P. and X.N.; Software, J.C.; Validation, J.C. and R.P.; Formal analysis, J.C. and X.N.; Investigation, J.C.; Resources, X.N.; Data curation, J.C.; Writing—original draft, J.C.; Writing—review & editing, J.C., R.P. and X.N.; Supervision, X.N.; Project administration, X.N.; Funding acquisition, X.N. All authors have read and agreed to the published version of the manuscript.

Funding: This research received no external funding.

Institutional Review Board Statement: Not applicable.

Informed Consent Statement: Not applicable.

Data Availability Statement: Data available upon request.

Acknowledgments: The authors wish to express special thanks to Christopher Thomson and Filipe Vilela, Institute of Chemistry Science, Heriot-Watt University for supplying photosensitizers, and the associated information for synthesis and characterization, as well as Andrew Haston for fabricating the LED baffles and Douglas Wagener for constructing the experimental rigs.

Conflicts of Interest: The authors have no conflicts interest regarding the work reported in this paper.

Nomenclature

| | |
|-------------------|--|
| $Area_{as}$ | integrated NMR area of ascaridole |
| $Area_{\alpha T}$ | integrated NMR area of α -terpinene |
| C_{as} | concentration of ascaridole (mol L^{-1}) |
| $C_{\alpha T}$ | concentration of α -terpinene (mol L^{-1}) |
| D | tube diameter (m) |
| f | oscillation frequency (Hz) |
| Re_o | oscillatory Reynolds number |
| St | Strouhal number |
| x_o | oscillatory center-to-peak amplitude (m) |
| ρ | density (kg m^{-3}) |

References

1. Buglioni, L.; Raymenants, F.; Slattery, A.; Zondag, S.D.A.; Noël, T. Technological innovations in photochemistry for organic synthesis: Flow chemistry, high-throughput experimentation, scale-up, and photoelectrochemistry. *Chem. Rev.* **2021**, *122*, 2752–2906. [[CrossRef](#)]
2. Ronzani, F.; Costarramone, N.; Blanc, S.; Benabbou, A.K.; Behec, M.L.; Pigot, T.; Oelgemöller, M.; Lacombe, S. Visible-light photosensitized oxidation of α -terpinene using novel silica-supported sensitizers: Photooxygenation vs. photodehydrogenation. *J. Catal.* **2013**, *303*, 164–174. [[CrossRef](#)]
3. Baptista, M.S.; Cadet, J.; Mascio, P.D.; Ghogare, A.A.; Greer, A.; Hamblin, M.R.; Lorente, C.; Nunez, S.C.; Ribeiro, M.S.; Thomas, A.H.; et al. Type I and type II photosensitized oxidation reactions: Guidelines and mechanistic pathways. *Photochem. Photobiol.* **2017**, *93*, 912–919. [[CrossRef](#)]
4. Zondag, S.D.A.; Mazzarella, D.; Noël, T. Scale-Up of Photochemical Reactions: Transitioning from Lab Scale to Industrial Production. *Annu. Rev. Chem. Biomol. Eng.* **2023**, *14*, 283–300. [[CrossRef](#)]
5. Kayahan, E.; Jacobs, M.; Braeken, L.; Thomassen, L.C.J.; Kuhn, S.; Gerven, T.V.; Leblebici, M.E. Dawn of a new era in industrial photochemistry: The scale-up of micro-and mesostructured photoreactors. *Beilstein J. Org. Chem.* **2020**, *16*, 2484–2504. [[CrossRef](#)]

6. Chaudhuri, A.; Kuijpers, K.P.L.; Hendrix, R.B.J.; Shivaprasad, P.; Hacking, J.A.; Emanuelsson, E.A.C.; Noël, T.; Schaaf, J.V.D. A kinetic study of a photo-oxidation reaction between α -terpinene and singlet oxygen in a novel oscillatory baffled photo reactor. *Chem. Eng. J.* **2020**, *400*.
7. Donnelly, K.; Baumann, M. Scalability of photochemical reactions in continuous flow model. *J. Flow Chem.* **2021**, *11*, 223–241. [[CrossRef](#)]
8. Lee, D.S.; Amara, Z.; Clark, C.A.; Xu, Z.; Kakimpa, B.; Morvan, H.P.; Pickering, T.J.; Poliakoff, M.; George, M.W. Continuous photo-oxidation in a vortex reactor: Efficient operations using air drawn from the laboratory. *Org. Process Res. Dev.* **2017**, *21*, 1042–1050. [[CrossRef](#)]
9. Tobin, J.M.; Liu, J.; Hayes, H.; Demleitner, M.; Ellis, D.; Arrighi, V.; Xu, Z.; Vilela, F. BODIPY-based conjugated microporous polymers as reusable heterogeneous photosensitisers in a photochemical flow reactor. *Polym. Chem.* **2016**, *7*, 6662–6670. [[CrossRef](#)]
10. Shvydkiv, O.; Jähnisch, K.; Steinfeldt, N.; Yavorsky, A.; Oelgemöller, M. Visible-light photooxygenation of α -terpinene in a falling film microreactor. *Catal. Today* **2018**, *308*, 102–118. [[CrossRef](#)]
11. Dong, Z.; Wen, Z.; Zhao, F.; Kuhn, S.; Noël, T. Scale-up of micro-and milli-reactors: An overview of strategies, design principles and applications. *Chem. Eng. Sci. X* **2021**, *10*, 100097. [[CrossRef](#)]
12. Su, Y.; Kuijpers, K.; Hessela, V.; Noël, T. A convenient numbering-up strategy for the scale-up of gas–liquid photoredox catalysis in flow. *React. Chem. Eng.* **2016**, *1*, 73–81. [[CrossRef](#)]
13. Kuijpers, K.P.L.; van Dijk, M.A.H.; Rumeur, Q.G.; Hessel, V.; Su, Y.; Noël, T. A sensitivity analysis of a numbered-up photomicroreactor system. *React. Chem. Eng.* **2017**, *2*, 109–115. [[CrossRef](#)]
14. Moschetta, E.G.; Richter, S.M.; Wittenberger, S.J. Heuristics, protocol, and considerations for flow chemistry in photoredox catalysis. *ChemPhotoChem* **2017**, *1*, 539–543. [[CrossRef](#)]
15. Taylor, G.I. Conditions under which dispersion of a solute in a stream of solvent can be used to measure molecular diffusion. *R. Soc.* **1954**, *225*, 473–477.
16. Taylor, G.I. Dispersion of soluble matter in solvent flowing slowly through a tube. *R. Soc.* **1953**, *219*, 186–203.
17. Ni, X. Photo reactor in WO2022013348A1, 2022. (Patent). Available online: <https://data.epo.org/gpi/EP4182069A1-PHOTO-REACTOR> (accessed on 15 January 2024).
18. Mackley, M.R.; Ni, X. Mixing and dispersion in a baffled tube for steady laminar and pulsatile flow. *Chem. Eng. Sci.* **1991**, *46*, 3139–3151. [[CrossRef](#)]
19. Ni, X.; Jian, H.; Fitch, A.W. Computational fluid dynamic modelling of flow patterns in an oscillatory baffled column. *Chem. Eng. Sci.* **2002**, *57*, 2849–2862. [[CrossRef](#)]
20. Ni, X.; Mackley, M.R.; Harvey, A.P.; Stonestreet, P.; Baird, M.H.I.; Rao, N.V.R. Mixing through oscillations and pulsations—A guide to achieving process enhancements in the chemical and process industries. *Chem. Eng. Res. Des.* **2003**, *81*, 373–383. [[CrossRef](#)]
21. Dickens, A.W.; Mackley, M.R.; Williams, H.R. Experimental residence time distribution measurements for unsteady flow in baffled tubes. *Chem. Eng. Sci.* **1989**, *44*, 1471–1479. [[CrossRef](#)]
22. Jian, H.; Ni, X. A numerical study on the scale-up behaviour in oscillatory baffled columns. *Chem. Eng. Res. Des.* **2005**, *83*, 1163–1170. [[CrossRef](#)]
23. Ni, X.; Gélécourt, Y.S.; Neil, J.; Howes, T. On the effect of tracer density on axial dispersion in a batch oscillatory baffled column. *Chem. Eng. J.* **2002**, *85*, 17–25. [[CrossRef](#)]
24. Jimeno, G.; Lee, Y.C.; Ni, X. The effect of particle size on flow in a continuous oscillatory baffled reactor using CFD. *Can. J. Chem. Eng.* **2021**, *100*, S258–S271. [[CrossRef](#)]
25. Jiang, M.; Ni, X. Reactive crystallization of paracetamol in a continuous oscillatory baffled reactor. *Org. Process Res. Dev.* **2019**, *23*, 882–890. [[CrossRef](#)]
26. NiTech. Available online: www.nitechsolutions.co.uk (accessed on 15 January 2024).
27. Burguete, M.I.; Galindo, F.; Gavara, R.; Luis, S.V.; Moreno, M.; Thomas, P.; Russell, D.A. Singlet oxygen generation using a porous monolithic polymer supported photosensitizer: Potential application to the photodynamic destruction of melanoma cells. *Photochem. Photobiol. Sci.* **2008**, *8*, 37–44. [[CrossRef](#)]
28. Fabregat, V.; Burguete, M.I.; Galindo, F.; Luis, S.V. Singlet oxygen generation by photoactive polymeric microparticles with enhanced aqueous compatibility. *Environ. Sci. Pollut. Res.* **2013**, *21*, 11884–11892. [[CrossRef](#)]
29. Aubry, J.M.; Mandard-Cazin, B.; Rougee, M.; Bensasson, R.V. Kinetic studies of singlet oxygen [4 + 2]-cycloadditions with cyclic 1, 3-dienes in 28 solvents. *J. Am. Chem. Soc.* **1995**, *117*, 9159–9164. [[CrossRef](#)]
30. Adam, W.; Prein, M. Diastereoselective [4 + 2] cycloaddition of singlet oxygen in the photooxygenation of chiral naphthyl alcohols: Evidence for a hydroxy group-directing effect. *J. Am. Chem. Soc.* **1993**, *115*, 3766–3767. [[CrossRef](#)]
31. Bauch, M.; Fudickar, W.; Linker, T. tereoselective [4 + 2] cycloaddition of singlet oxygen to naphthalenes controlled by carbohydrates. *Molecules* **2021**, *26*, 804. [[CrossRef](#)]
32. Ghogare, A.A.; Greer, G. Using singlet oxygen to synthesize natural products and drugs. *Chem. Rev.* **2016**, *116*, 9994–10034. [[CrossRef](#)]
33. Villén, L.; Manjón, F.; García-Fresnadillo, D.; Orellana, G. Solar water disinfection by photocatalytic singlet oxygen production in heterogeneous medium. *Appl. Catal. B Environ.* **2006**, *69*, 1–9. [[CrossRef](#)]
34. Rodgers, M.A.J. *NATO ASI Series A; Life Sciences*; LENUM Publishing Corporation: New York, NY, USA, 1984; Volume 85.

35. Ogilby, P.R.; Foote, C.S. Chemistry of singlet oxygen. 42. Effect of solvent, solvent isotopic substitution, and temperature on the lifetime of singlet molecular oxygen (1. DELTA. g). *J. Am. Chem. Soc.* **1983**, *105*, 3423–3430. [[CrossRef](#)]
36. Gianotti, E.; Estevão, B.M.; Cucinotta, F.; Hioka, N.; Rizzi, M.; Renò, F.; Marchese, L. An Efficient Rose Bengal Based Nanoplatforam for Photodynamic Therapy. *Chem. Eur. J.* **2014**, *20*, 10921–10925; [[CrossRef](#)] [[PubMed](#)]
37. Whitmire, C. *Photosensitizers: Types, Uses and Selected Research*; Nova Science Publishers: Hauppauge, NY, USA, 2016.
38. Deshpande, M.S.; Rale, V.B.; Lynch, J.M. Aureobasidium pullulans in applied microbiology: A status report. *Enzym. Microb. Technol.* **1992**, *14*, 514–527. [[CrossRef](#)]
39. Wong, Y.L.; Tobin, J.M.; Xua, Z.; Vilela, F. Conjugated porous polymers for photocatalytic applications. *J. Mater. Chem. A* **2016**, *4*, 18677–18686. [[CrossRef](#)]
40. Zhang, K.; Kopetzki, D.; Seeberger, P.H.; Antonietti, M.; Vilela, F. Surface area control and photocatalytic activity of conjugated microporous poly (benzothiadiazole) networks. *Angew. Chem. Int. Ed. Engl.* **2013**, *52*, 1432–1436. [[CrossRef](#)]
41. Elvira, K.S.; Wootton, R.C.R.; Reis, N.M.; Mackley, M.R.; de Mello, A.J. Through-wall mass transport as a modality for safe generation of singlet oxygen in continuous flows. *ACS Sustain. Chem. Eng.* **2013**, *1*, 209–213. [[CrossRef](#)]
42. Shen, J.; Steinbach, R.R.; Tobin, J.; Nakata, M.M.; Bower, M.; McCoustra, M.R.S.; Bridle, H.; Arrighi, V.; Vilela, F. Photoactive and metal-free polyamide-based polymers for water and wastewater treatment under visible light irradiation. *Appl. Catal. B Environ.* **2016**, *193*, 226–233. [[CrossRef](#)]
43. Thomson, C.G.; Jones, C.M.S.; Rosair, G.; Ellis, D.D.; Hueso, J.M.; Lee, A.L.; Vilela, F. Continuous-flow synthesis and application of polymer-supported BODIPY Photosensitisers for the generation of singlet oxygen; process optimised by in-line NMR spectroscopy. *J. Flow Chem.* **2020**, *10*, 327–345. [[CrossRef](#)]
44. Hoops, S.; Sahle, S.; Gauges, R.; Lee, C.; Pahle, J.; Simus, N.; Singhal, M.; Xu, L.; Mendes, P.; Kummer, U. COPASI—A complex pathway simulator. *Bioinformatics* **2006**, *22*, 3067–3074. [[CrossRef](#)]
45. Alofi, S.; O'Rourke, C.; Mills, A. Kinetics of stearic acid destruction on TiO₂ 'self-cleaning' films revisited. *Photochem. Photobiol. Sci.* **2022**, *21*, 2061–2069. [[CrossRef](#)]
46. Luke, L.V.; Rickenbach, S.S.; McCormick, T.M. Singlet oxygen quantum yields determined by oxygen consumption. *J. Photochem. Photobiol. A Chem.* **2019**, *378*, 131–135.
47. Erickson, P.R.; Moor, K.J.; Werner, J.J.; Latch, D.E.; Arnold, W.A.; McNeill, K. Singlet oxygen phosphorescence as a probe for triplet-state dissolved organic matter reactivity. *Environ. Sci. Technol.* **2018**, *52*, 9170–9178. [[CrossRef](#)]
48. Hockey, R.M.; Nouri, J.M. Turbulent flow in a baffled vessel stirred by a 60 pitched blade impeller. *Chem. Eng. Sci.* **1996**, *51*, 4405–4421. [[CrossRef](#)]
49. Zhao, J.; Wu, W.; Suna, J.; Guo, S. Triplet photosensitizers: From molecular design to applications. *Chem. Soc. Rev.* **2013**, *42*, 5323–5351. [[CrossRef](#)]
50. Midden, W.R.; Wang, S.Y. Singlet oxygen generation for solution kinetics: Clean and simple. *Am. Chem. Soc.* **1983**, *105*, 4129–4135. [[CrossRef](#)]
51. Sunday, M.O.; Sakugawa, H. A simple, inexpensive method for gas-phase singlet oxygen generation from sensitizer-impregnated filters: Potential application to bacteria/virus inactivation and pollutant degradation. *Sci. Total Environ.* **2020**, *746*, 141186. [[CrossRef](#)]
52. Oliveira, M.S.N.; Ni, X. Characterization of a gas-liquid OBC: Bubble size and gas holdup. *AIChE J.* **2004**, *50*, 3019–3033. [[CrossRef](#)]
53. Ahmed, S.M.R.; Phan, A.N.; Harvey, A.P. Scale-up of oscillatory helical baffled reactors based on residence time distribution. *Chem. Eng. Technol.* **2017**, *40*, 907–914. [[CrossRef](#)]

Disclaimer/Publisher's Note: The statements, opinions and data contained in all publications are solely those of the individual author(s) and contributor(s) and not of MDPI and/or the editor(s). MDPI and/or the editor(s) disclaim responsibility for any injury to people or property resulting from any ideas, methods, instructions or products referred to in the content.